scientific reports

Check for updates

OPEN

A gelable polymer loaded with curcumin and apatinib absorbed in gelatin sponge delays postoperative residual tumor growth

Zhuo-Nan Meng[1,9], Jian-Yuan Chen[1,9], Chong Yu[2], Ai-hong Zheng[3], O. Sreekanth Reddy[2], Kai-Yan Liu[2], Yong-Rui Su[1], Shi-Tai Zhang[1], Yin-Shuang Wang[4], Hang-Yu Gu[5], Fu-Wei Wang[3], Song-Cheng Xu[6], Li-Tao Sun[6], Bing-Chen Chen[7], Wing-Fu Lai[2,8]✉, Guo-Qing Wu[3]✉ & Da-Hong Zhang[2]✉

Surgical resection of the tumor remains the preferred treatment for most solid tumors at an early stage, however, residual tumor cells after surgical resection poses a considerable obstacle in cancer treatment. Here, we developed a gel carrier using a cellulose-based gel-forming polymer (CT) combined with gelatin sponge (GS) to fill the resection cavity and delay postoperative residual tumor growth. The fabricated gel exhibited a porous nature along with gradual swelling and erosion over time. Curcumin (Cur) and apatinib (Apa) were loaded into CT gel (CT-CA), and a sustained release behavior was observed at pH 7.4 and 6.4 at 37 °C. The preclinical studies indicated that the mouse weight and tissue exhibited no apparent change after administration of the GS-CT compared with the control. The in vivo fluorescence images showed that GS-CT has the capability to regulate the release of Cur and Apa, facilitating the accumulation of these two agents at the surgical tumor site. Moreover, GS-CT loaded Cur and Apa (GS-CT-CA) delayed postoperative residual tumor growth in intraperitoneal and subcutaneous postoperative mouse models. These findings demonstrated that our gel carrier system significantly prevents postoperative residual tumor growth because of enhanced drug accumulation and sustained drug release at the tumor site.

Keywords Curcumin, Apatinib, Gelatin sponge, Gel-forming polymer, Postoperative residual tumor

Cancer ranks as the second-leading cause of global mortality and remains a significant public health issue worldwide[1]. Despite the rapid advancements in pharmaceuticals and radiotherapy, surgical resection continues to be the most preferred treatment, particularly for solid malignancies in their early stages[2–4]. Clinical evidence indicates that solid tumors often exhibit a high degree of invasiveness. Even after aggressive resection, some small tumor cells may remain, which can lead to tumor implantation at the surgical site and significantly increase the risk of local recurrence[5–7]. Furthermore, extensive removal of healthy tissue around the tumor can greatly disrupt the structural and functional integrity of the original organ and tissue, potentially resulting in

[1]The Second Clinical Medical College, Zhejiang Chinese Medical University, Hangzhou, Zhejiang, China. [2]Department of Urology, Urology & Nephrology Center, Zhejiang Provincial People'sHospital, Affiliated People's Hospital, Hangzhou Medical College, No. 138 ShangTang Road, Hangzhou 310014, China. [3]Department of Medical Oncology, Cancer Center, Zhejiang Provincial People's Hospital(Affiliated People's Hospital, Hangzhou Medical College), No. 138 ShangTang Road, Hangzhou 310014, China. [4]Department of Ultrasound Medicine, The First Affiliated Hospital of Ningbo University, Ningbo 315010, Zhejiang Province, China. [5]Department of Oncology and Hematology, Beilun District People's Hospital, Ningbo, China. [6]Department of Ultrasound, Zhejiang Provincial People's Hospital (Affiliated People'sHospital, Hangzhou Medical College), No. 138 ShangTang Road, Hangzhou 310014, China. [7]Department of Anal Surgery, Zhejiang Provincial People's Hospital (Affiliated People's Hospital, Hangzhou Medical College), Hangzhou, China. [8]School of Food Science and Nutrition, University of Leeds, Leeds LS29JT, UK. [9]Zhuo-Nan Meng and Jian-Yuan Chen contributed equally to this work. ✉email: rori0610@graduate.hku.hk; gqwuzsu@hotmail.com; zhangdahong168@163.com

postoperative complications such as bleeding and infection. Therefore, there is a need to develop new implant materials that can achieve rapid hemostasis and prevent postoperative residual tumor growth.

Gelatin sponge is one of the most popular materials for hemostasis in clinical treatment[8]. It has strong absorption capacity and good physical pressure at the tumor site after surgery; it can achieve rapid hemostasis[9]. Also, it has positron attachment that facilitates platelet adhesion and local thrombus development, resulting in hemostatic action[10]. Previous studies have reported the gelatin sponge is biocompatible, flexible, biodegradable, and showed hemostatic activity[11–13]. It is proposed that gelatin sponge could increase the antitumor efficacy of drugs by facilitating drugs accumulation, owing to its capacity of absorbing the liquid at the surgical site and control hemorrhage.

Curcumin is an important Chinese herbal medicine, with great antitumor function that has been found for years[14]. It can reshape the tumor immune microenvironment through regulating the expression of molecules like P53[15], B-cell lymphoma 2, epidermal growth factor receptor, and Programmed cell Death ligand 1[16]. At the cellular level, it suppresses the activity of $CD4^{+}CD25^{+}$ Treg cells thereby enhancing the immune-stimulating effects of natural killer cells[17,18]. Besides, it could directly block the cell cycle, induce apoptosis, inhibit tumor invasion or metastasis[19,20]. However, one drawback of curcumin is its limited solubility in water. Pharmacokinetic data from animal experiments suggest poor absorption and rapid metabolism[21], which justifies local delivery of curcumin in cancer therapy. Apatinib is a novel, small-molecule, selective tyrosine kinase inhibitor that targets various tumor-related kinases, including vascular endothelial growth factor receptor-2. However, the currently available oral formulation, apatinib mesylate tablets, necessitates high clinical doses and is associated with significant side effects. To develop an efficient local delivery and controlled-release of Cur and Apa, gelatin sponge combined with cellulose-based gel-forming polymer (CT) loaded with Cur and Apa was prepared. Moreover, the maintenance of this efficacy enables a reduction in the clinical dosage of apatinib, thereby diminishing the occurrence of adverse reactions.

Materials and methods

Materials

2-methylpropenoic acid, 4-dimethylaminopyridine (DMAP), and 1-chloro-2,3-epoxypropane chemicals were purchased from Sigma-Aldrich (St. Louis, MO, USA). DMSO was purchased from Sigma-Aldrich (St. Louis, MO, USA). Curcumin was obtained from Sigma-Aldrich (St. Louis, MO, USA). Apatinib was donated by Hengrui Pharmaceuticals. (Jiangsu, China). The anti-CD8 alpha antibody (EPR21769) was purchased from Abcam (Cambridge, UK). DiR' [DiIC18(7)] was purchased from Aladdin (Shanghai, China).

CT synthesis and gel fabrication

2-methylpropenoic acid, 4-dimethylaminopyridine (DMAP), 1-chloro-2,3-epoxypropane, and various other chemicals were purchased from Sigma-Aldrich (St. Louis, MO, USA). CT was synthesized as previously described from modified cellulose (degree of hydroxypropylation = 7–12%; degree of methylation = 28–30%) whose 2% (w/v) aqueous solution exhibited the viscosity of 6 mPa·s at ambient conditions[22]. Gelation of CT was achieved by first dispersing the polymer, at a concentration of 1% (w/v), in an anhydrous drug-loaded DMSO solution. The solution was then added to 50 mL of distilled water. The gel was generated after incubation of the solution at ambient conditions for 10 min.

Morphological examination

The CT-based formulation was lyophilized, sectioned and sputter-coated with gold. The morphological features were observed by using a scanning electron microscope (JSM-6380; JEOL, Tokyo, Japan) operated at an accelerating voltage of 10 kV.

Determination of the water content

A lyophilized gel was weighed and immersed in 100 mL of PBS (pH 7.4). The gel was extracted using centrifugation, with a relative centrifugal force of 4000 × g and at 5-minute intervals. Extra PBS was removed from the gel using blotting. An equation was utilized to determine the water content of the gel:

$$Water\ content\ (\%) = \frac{m_s - m_d}{m_s} \times 100\%$$

where m_s is the mass of the swollen gel, and m_d is the mass of the dried gel.

Evaluation of the erosion behavior

The erosion behaviour of the gel was evaluated as previously reported[23]. Throughout the experiment, a specified quantity of freeze-dried gel was placed into PBS with a pH of 7.4. The system was then allowed to incubate at a temperature of 37 °C. Following a specific duration, the gel was retrieved through centrifugation at a relative centrifugal force of 4000 × g for 5 min. Subsequently, it was subjected to drying in an oven at 65 °C. Then the dry mass of the gel was recorded.

Preparation of Cur/Apa-loaded gels

Cur [4% (w/v)] and Apa [2% (w/v)] were added to 25 mL of a 5% (w/v) CT solution in DMSO, followed by magnetic stirring at ambient conditions for 30 min. The mixture was then added to distilled water and incubated for 10 min to induce gelation. After incubation, the system was centrifuged at 10,000 × g for 30 min. The supernatant was removed, and the Cur/Apa- loaded CT was obtained after freeze-drying. Similarly, the drug-loaded CT solution was transferred to a gelatin sponge and placed it in distilled water for 10 min to induce

gelation of CT in the gelatin sponge and then freeze-dried to get a gelatin-CT gel. A drug-loaded gelatin sponge was created by adding the drug solution to gelatin and incubating it overnight, followed by washing it with water and then freeze-dried it for 3 days.

Evaluation of encapsulation efficiency (EE)

Briefly, 0.2 g of Cur and 0.1 g of Apa was blended with 10mL of a 5% CT solution in DMSO. The homogenous solution was transferred through a syringe into 30 mL of water to form a gel. The obtained gel was centrifuged at 10,000 x g and freeze-dried for 3 days. Afterwards, 200 mg of gel was soaked in 30 mL of phosphate buffer saline for overnight. After that, the solution was crushed and subjected to sonication for 30 min, filtered, and analyzed at a wavelength of 430 for Cur and 340 for Apa. The encapsulation efficiency was calculated using the following formula as previously reported[24]:

$$\%\mathrm{EE} = \frac{\text{amount of drug in filtrate}}{\text{amount of drug added during preparation}}$$

Evaluation of in vitro release and kinetic studies

To understand the release behavior of drug-loaded carriers at different pH values (7.4 and 6.4), 100 mg of drug-loaded gel was suspended in 40 mL of PBS (pH 7.4 and 6.4) at 37 °C. At predetermined intervals of time, 4 mL of sample was withdrawn and analyzed using a UV-visible spectrophotometer at a fixed wavelength of 430 for Cur and 340 for Apa. The withdrawn media was replenished with the same volume of PBS to maintain sink conditions. To determine the release kinetics of the drug-loaded carriers, the release profiles were fitted into various kinetic models such as zero-order, first-order, and Higuchi. Furthermore, to evaluate the release mechanism, the release profiles were fitted into the Korsmeyer-Peppas model.

Mice

Eight-week-old C57BL/6 male mice weighing 20–25 g were purchased from Shanghai Slack Laboratory Animal Co., Ltd. (Shanghai, China). All animal procedures were approved by the Ethics Committee for Care and Use of Laboratory Animals of the Zhejiang Provincial People's Hospital (SCXK2017-0005) was conducted in accordance with the ARRIVE guidelines related to animal handling.

In vivo safety evaluation

Six healthy male C57BL/6 mice were randomly divided into two groups (control group and GS-CT group) for in vivo safety evaluation. The mice were housed individually in a temperature-controlled environment with a 12-hour light-dark cycle, with free access to food and water, and regular bedding changes. Anesthesia was administered using 1–1.5% isoflurane, and a midline abdominal incision was made to access the peritoneal cavity. The test material (GS-CT) was placed subperitoneally, followed by suturing of the incision. Postoperatively, the mice were kept warm and received standard care. They were monitored at predetermined intervals for their overall status, and body weight was recorded regularly.

In vivo fluorescence images

MB49 cells were subcutaneously injected into the peritoneum of C57BL/6 mice to establish the MB49 tumor-bearing mouse model. Once the tumor volume reached approximately 100 mm^3, tumor resection was performed. Following resection, DiR-GS and DiR-GS-CT were implanted at the tumor resection site. Fluorescence imaging was conducted using the IVIS® Lumina LT Series III system (PerkinElmer Medical Diagnostics Products, Shanghai, USA) to monitor drug release and distribution at the tumor site.

Treatment of tumor recurrence with GS-CT-CA in intraperitoneal and subcutaneous tumor model

A MB49 tumor-bearing mouse model was established by injecting MB49 cells into the left peritoneal wall of 8-week-old C57BL/6 mice. When the tumor volume reached approximately 100 mm^3, the mice were randomly divided into five groups for tumor resection, with each group receiving the following treatment post-resection: Blank: Tumor resection only. GS-CT: A gelatin sponge containing 100 μL of CT. GS-CT-D: A gelatin sponge containing 100 μL CT and DMSO. GS-CA: A gelatin sponge containing 100 μL of Cur (250 mg/kg) and Apa (100 mg/kg). GS-CT-CA: A gelatin sponge containing 100 μL of CT, Cur (250 mg/kg), and Apa (100 mg/kg) polymer. After the initial treatment, tumor recurrence was monitored every two days by checking for subcutaneous nodules in the peritoneal region. The time of tumor recurrence was recorded upon detection of noticeable subcutaneous nodules in the peritoneal area. Throughout the study, body weight was monitored, and on day 16, the mice were euthanized in a high concentration of carbon dioxide for further tumor tissue analysis.

For the subcutaneous tumor model, MB49 cells were injected into the left flank of 8-week-old C57BL/6 mice to validate the findings from the subcutaneous model. Since the peritoneal model showed that DMSO had minimal impact on the results, only four groups were tested in this model: Blank control, GS-CT, GS-CA, and GS-CT-CA. The experimental procedures were conducted similarly to the peritoneal model described above.

H&E and IHC

Tumor tissue obtained from the in vivo antitumor recurrence studies was embedded in paraffin for histological analysis. Sections of 3–4 micrometers were cut and stained with hematoxylin and eosin (H&E) for general tissue structure examination. For immunofluorescence analysis, 5-micrometer sections were prepared, dried at 65 °C for 1 h, and then dewaxed by incubation in 95 °C Tris/EDTA buffer for 20 min. After dewaxing and hydration, antigen retrieval was performed. Next, the sections were incubated with 5% goat serum for 15 min

to block endogenous peroxidase activity. The sections were then incubated overnight at 4 °C with rabbit anti-mouse CD8α (1:2000, Abcam). The following day, the sections were incubated with goat anti-rabbit HRP (1:50, Beyotime) at room temperature for 30 min. Visualization was achieved using 3,3′-diaminobenzidine (DAB) as the chromogen, and the slides were counterstained with hematoxylin. Quantification of staining intensity was performed using ImageJ software.

Statistical analysis

A paired t test or Wilcoxon rank-sum test was used for two-sample comparisons, depending on data distribution Graphs were generated using Prism 8.0, and a P value of < 0.05 was considered statistically significant.

Results and discussion

Gel preparation and characterization

The initial stages of creating CT involve hydroxypropylation and methylation of cellulose, followed by transesterification facilitated by a polar aprotic solvent as the reaction medium. The scanning electron microscope (SEM) was utilized to examine the microstructure of the CT-based gel formulation upon lyophilization (Fig. 1). Entanglement of the polymeric molecules results in the formation of a dense gel structure. The porous microstructure will be utilized to trap Cur and Apa over time, enabling their sustained release, with the aim of enhancing the efficacy of the regimen for subsequent prevention of postoperative tumor recurrence. Furthermore, the SEM images reveal that the outer surface of the gelatin sponge shows a highly porous nature; after the incorporation of CT-gel into the gelatin sponge, a dense structure with a less porous nature was observed. Compared to CT gel, the gelatin-CT gel has a low degree of porous nature; hence, the trapped molecules inside the gelatin-CT gel can diffuse out slowly compared to that in CT gel (Fig. 2).

In addition, this porous network of polymeric molecules is anticipated to lead to gradual swelling and erosion of the gel as time passes, thus facilitating sustained release of the therapeutic agent for subsequent phases of this investigation. Prior studies have already shown that the release sustainability of the gel can be influenced by the swelling and erosion characteristics, as well as the water solubility of the loaded agent[25–28]. The latter is elucidated by the notion that Fickian diffusion, predominantly governed by the extent of gel swelling, generally facilitates the release of the encapsulated agent from a matrix-type drug delivery system[29–32]. The gel network of polymeric molecules, created through molecular entanglement, facilitates slow swelling and erosion over time (Fig. 3).

Drug release and kinetics studies

The EE of Cur and Apa in CT-CA gel, gelatin, and gelatin-CT gel are 55.9,44.75, 49.28, 42.05, 66.6, and 53.3%respectively. The amount of drug molecules encapsulated in the polymer matrix depends on the solubility and the molecular weight of the drug substances; both drugs (Cur and Apa) used in the present study are hydrophobic, hence the % EE has lowered. The release pattern of CT-CA is examined at pH 6.4 and 7.4, and the results revealed that at both pH levels, the gel carriers showed sustained and lower release rate (Fig. 4). This is due to poor aqueous solubility of loaded agents; furthermore, the high mechanical integrity and stability of gel lead to a lower release rate. Furthermore, it is observed that after the incorporation of CT-gel into the gelatin sponge, the initial burst release was lowered compared to CT-gel because the gelatin sponge can act as a barrier to expose the gel to the PBS medium; thereby, the rate of water influx decreases, and consequently, the diffusion of the drug molecules decreases; hence, the initial burst release was lowered. To understand the release kinetics and mechanism of drug-loaded carriers, the release data were fitted into various models such as zero-order, first-order, Higuchi, and Korsmeyer-Peppas and the results are presented in Table 1. The correlation coefficient (r^2) values are closer to Higuchi model, indicating that the drug molecules release from the polymer matrix via a diffusion mechanism and increase the release rate as time goes on. Furthermore, from the Korsmeyer-Peppas results, the n values lie between 0.392 and 0.666; therefore, the release mechanism follows the Fickian-to-non-Fickian mechanism. This implies that the release of drugs from developed gels is primarily due to the diffusion process followed by the relaxation of the polymer matrix.

In vivo safety evaluation

The in vivo safety of the GS-CT material was evaluated through subperitoneal implantation of GS-CT in healthy C57BL/6 mice, monitored the body weight of mice for 16 days post-implantation and the results are presented in Fig. 5A. The findings demonstrated that body weight had increased in both GS-CT and control groups, suggesting the biocompatibility of GS-CT material. Furthermore, the histological changes in the heart, liver, spleen, lungs, and kidneys were evaluated by H&E staining, and the results are depicted in Fig. 5B. Similar to the control group, no morphological changes were noted in the organs subjected to GS-CT treatment, indicating no detectable toxicity.

In vivo fluorescence images

Drug concentration at the therapeutic site and sustained release are crucial factors for effective inhibition of tumor growth[33]. In order to monitor the dynamic release and distribution of drugs in vivo, we used a near-infrared dye, DiR that has a similar solubility to that of Cur, to simulate GS-CT-CA and GS-CA (Fig. 5C). The results demonstrated that both formulations, DiR-GS-CA and DiR-GS-CT-CA, exhibited sharp fluorescence intensity signal on day 1. The fluorescence intensity signal of DiR-GS-CT-CA reduced slightly at 7 days after implantation, while DiR-GS-CA showed significant reduction compared to DiR-GS-CT-CA. At 14 days after implantation, the signal intensity was very weak in DiR-GS-CA and no signal was observed at 21 days. On the contrary, the signal intensity of DiR-GS-CT-CA was still clearly observed at 21 days after implantation. This suggests that fluorescence decayed much slower in mice implanted with DiR-GS-CT-CA compared to those

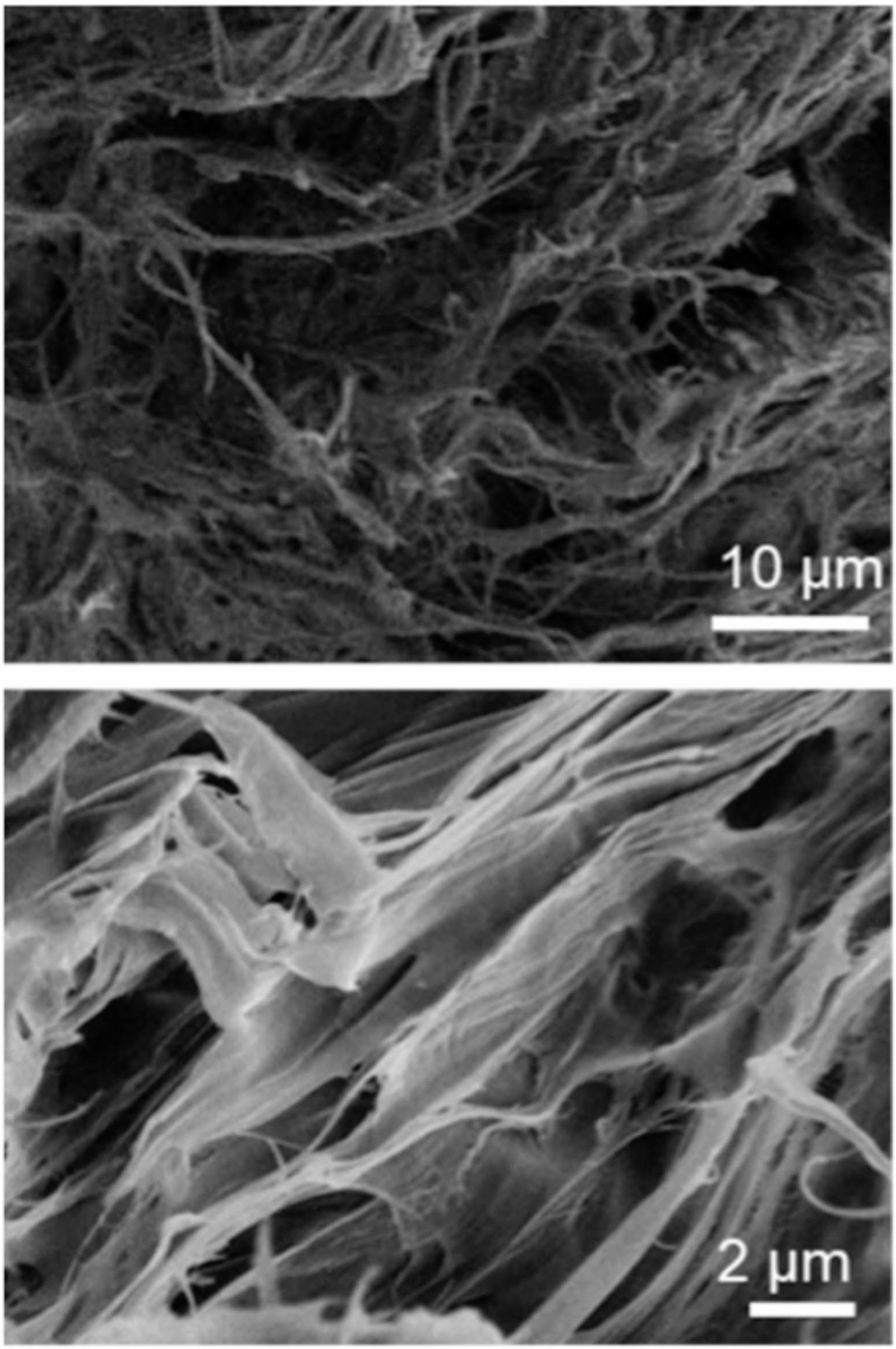

Fig. 1. SEM micrographs, with different degrees of magnification, showing the microstructure of the CT-based formulation.

implanted with DiR-GS-CA. Hence, CT was able to mediate drug accumulation and sustained release of loaded agents in mouse models.

GS-CT-CA delayed postoperative residual tumor growth in the intraperitoneal tumor model

An intraperitoneal residual tumor model was established using MB49 cells to assess the efficacy of GS-CT-CA in delaying residual tumor growth. Specifically, when the tumor had grown approximately 10 mm in diameter,

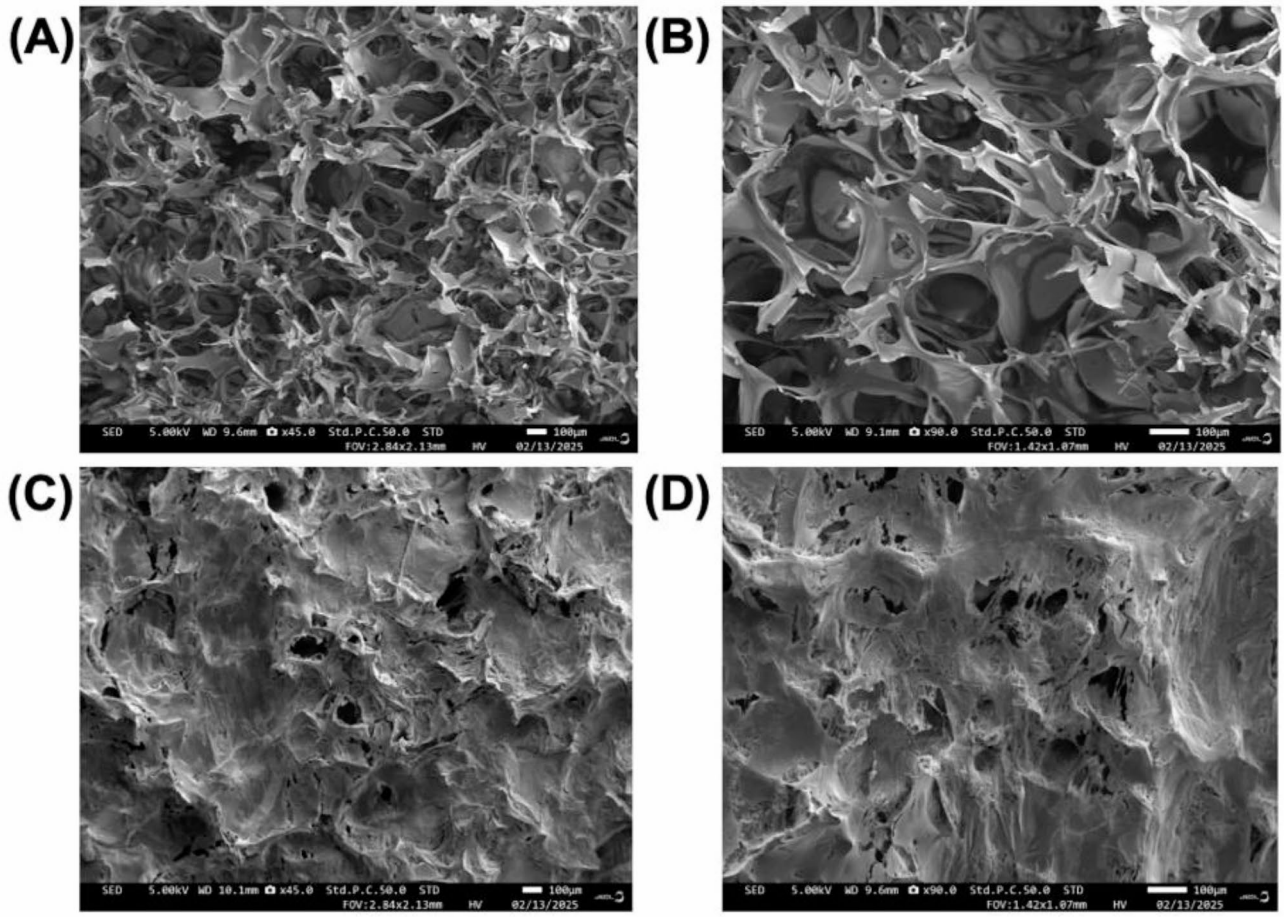

Fig. 2. SEM micrographs of gelatin sponge (**A** & **B**) and gelatin-CT (**C** & **D**).

it was resected using traditional surgical techniques, with a residual tumor of 1 mm in diameter to simulate the positive surgical margins. After tumor resection, GS-CT-CA was then implanted at the tumor site, the surgical steps from tumor resection to material implantation were shown in Fig. 6A. Thereafter, the tumor growth in mice treated with different agents and/or carriers were recorded. As depicted in Fig. 6B, the blank group exhibited a 100% tumor reoccurrence rate on day 6 (post-operation), while the GS-CT reached 100% tumor reoccurrence rate on day10, indicating that GS-CT alone exhibited slight inhibition activity. However, the tumor reoccurrence rate of GS-CT-CA was 20% on day 8 and reached 100% on day 16. After 16 days, the blank group was euthanized due to excessive tumor burden in one of the mice, in accordance with animal ethics requirements. The mice implanted with GS-CT-CA had the least tumor volumes and tumor weight among all groups (Fig. 6C,D). In addition, the body weight of mice in the GS-CT-CA group was significantly greater than that in the blank group (Fig. 6E), indicating a healthier status in mice treated with GS-CT-CA. Histological analysis of the tumor tissue was performed at the end of the treatment to investigate the mechanisms underlying tumor growth delay. Pathologically, the H&E staining results showed that, compared to mice in other groups, the mice in GS-CT-CA group had more pronounced tumor areas with necrosis (Fig. 6F, top panel). Further immunohistochemical staining using the αCD8 revealed a significant increase in $CD8^+$ T cells in tumors from the GS-CT-CA group compared to those in other groups (Fig. 6F, bottom panel and Fig. 6G), implying that $CD8^+$ T cells mediated tumor growth delay in GS-CT-CA group. Taken together, these findings suggested that GS-CT-CA had the strongest ability to delay residual tumor growth in our intraperitoneal residual tumor model, and the underlying mechanism might involve inducing tumor cell necrosis and facilitating $CD8^+$ T cell infiltration into tumor tissues.

GS-CT-CA delayed postoperative residual tumor growth in the subcutaneous tumor model

In an intraperitoneal residual tumor model, GS-CT-CA demonstrated a significant delay effect on postoperative residual tumor growth. To further validate these findings, a subcutaneous residual tumor model was established. Consistently, GS-CT-CA group had minimal tumor growth compared to the other groups and demonstrated the lowest reoccurrence rate across all time points. On day 16, mice in GS-CT-CA group exhibited an 80% tumor reoccurrence rate, in contrast to the 100% reoccurrence rate observed in the other groups (Fig. 7A). The tumor size and weight in the GS-CT-CA group were the smallest among all the groups (Fig. 7B,C). At the end of the experiment, mice from GS-CT-CA group gained more body weight than those in the other groups (Fig. 7D).

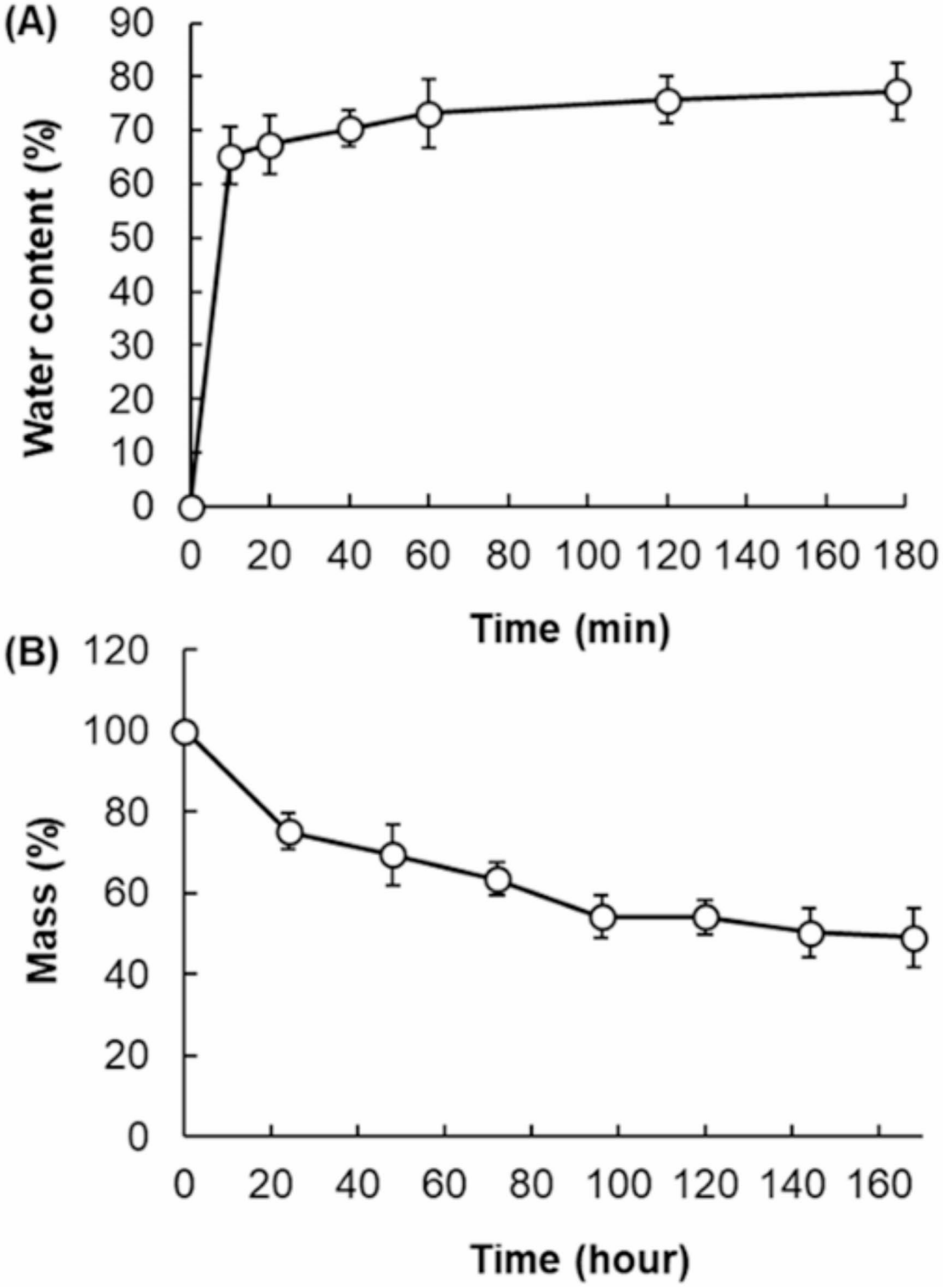

Fig. 3. Swelling capacity and erosion susceptibility of the CT-based formulation.

A reminiscence of the findings in the retroperitoneal model, H&E staining and immunohistochemistry assays revealed that the elevated necrosis areas and an increased presence of $CD8^+$ T cells were observed in tumor tissues from mice treated with GS-CT-CA (Fig. 7E,F). These results further confirmed the efficacy of GS-CT-CA effectively delayed postoperative residual tumor growth.

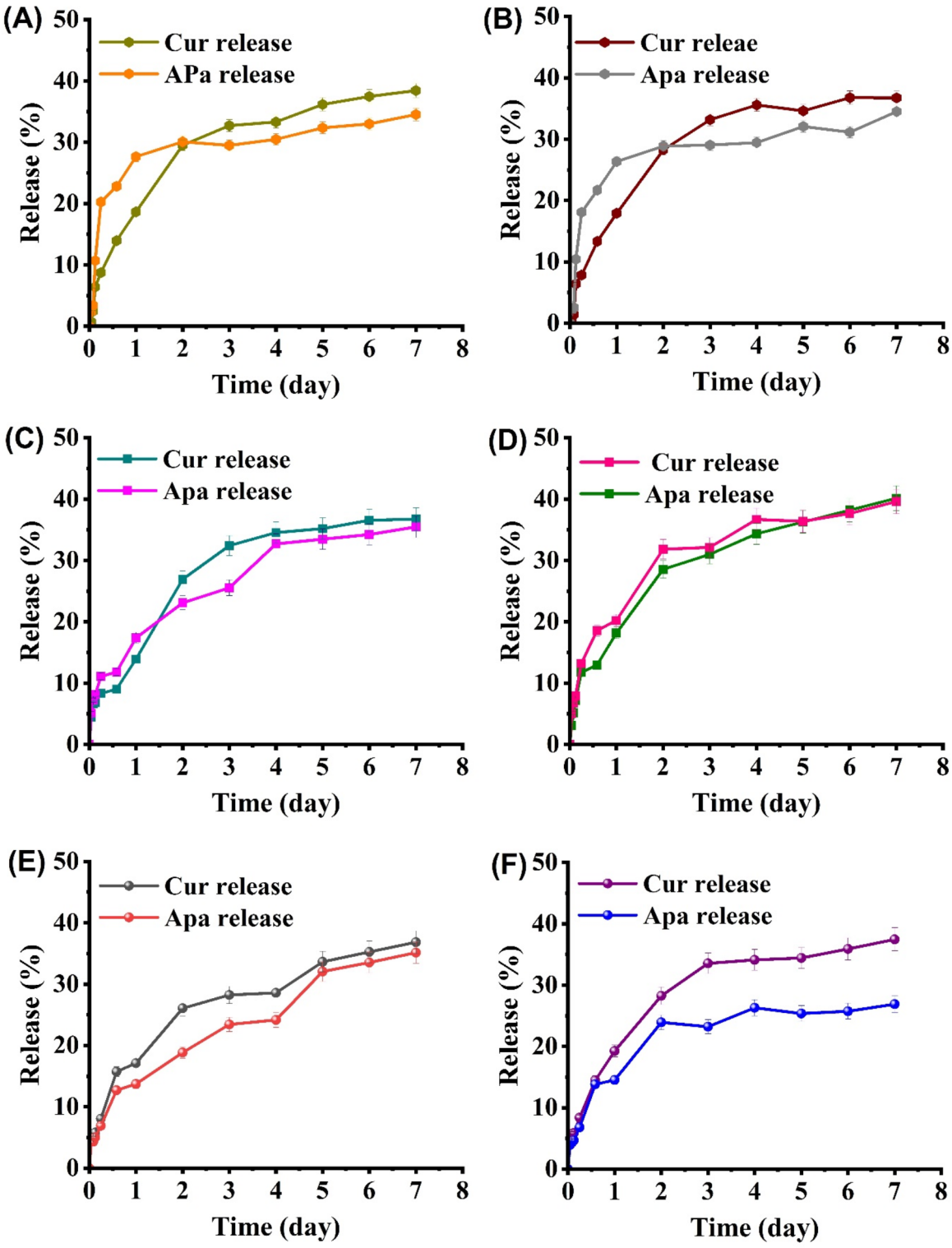

Fig. 4. Release profiles of Cur and Apa from CT gel in pH 6.4 (**A**) and 7.4 (**B**); gelatin sponge in pH 6.4 (**C**) and 7.4 (**D**); gelatin-CT gel in pH 6.4 (**E**) and 7.4 (**F**) at 37 °C.

Conclusions

By using gel-forming non-conjugated polymers combined with gelatin sponges, we successfully delivered curcumin and apatinib to tumor sites and delayed postoperative residual tumor growth. The present study concluded that CT combined with gelatin sponges is an effective and safe drug local delivery system. This drug delivery system is able to mediate controlled-drug release. When loaded with curcumin and apatinib, this drug

Code	Drug	pH	Zero-order		First-order		Higuchi		Korsmeyer-Peppas	
			K_0	r^2	K_1	r^2	K_H	r^2	n	r^2
CT-CA	Cur	7.4	7.133	0.774	0.096	0.481	16.371	0.924	0.666	0.978
		6.4	7.263	0.787	0.098	0.490	16.671	0.930	0.649	0.983
CT-CA	Apa	7.4	6.562	0.596	0.087	0.376	15.648	0.616	0.418	0.878
		6.4	6.737	0.568	0.090	0.370	16.139	0.550	0.404	0.869
Gelatin	Cur	7.4	7.186	0.619	0.095	0.736	16.580	0.967	0.484	0.980
		6.4	6.868	0.652	0.090	0.760	15.779	0.949	0.582	0.951
Gelatin	Apa	7.4	7.321	0.364	0.099	0.529	17.165	0.899	0.418	0.974
		6.4	6.491	0.480	0.083	0.605	15.076	0.931	0.392	0.948
Gelatin-CT	Cur	7.4	6.938	0.517	0.091	0.651	16.143	0.935	0.516	0.994
		6.4	6.540	0.586	0.084	0.693	15.115	0.960	0.464	0.981
Gelatin-CT	Apa	7.4	5.108	0.344	0.062	0.455	12.021	0.872	0.462	0.957
		6.4	6.038	0.735	0.075	0.805	13.751	0.977	0.505	0.973

Table 1. Drug release kinetics of cur and apa of CT-CA were analyzed in pH 7.4 and 6.4 at 37 °C.

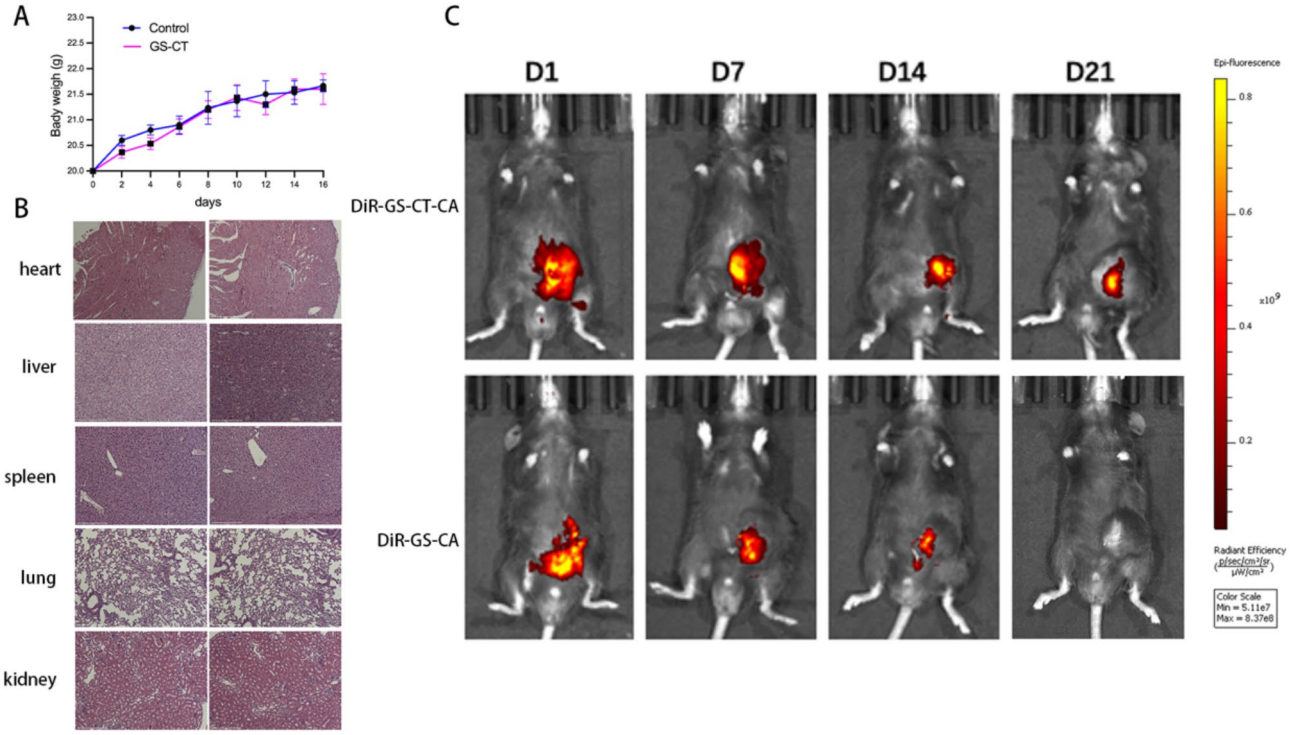

Fig. 5. In vivo safety evaluation and fluorescence images. (**A**) Body weight curves of mice after implantation with control and GS-CT. (Control: healthy mice with no implantation). (**B**) H&E staining of the mice organs (heart, liver, spleen, lung, and kidney) treated with control and GS-CT over 16 days of implantation. (**C**) Fluorescence imaging of mice treated with DiR-GS-CA and DiR-GS-CT-CA.

delivery system can delay postoperative residual tumor growth and delay tumor reoccurrence. Further clinical studies are warranted to explore whether it can prevent postoperative tumor recurrence.

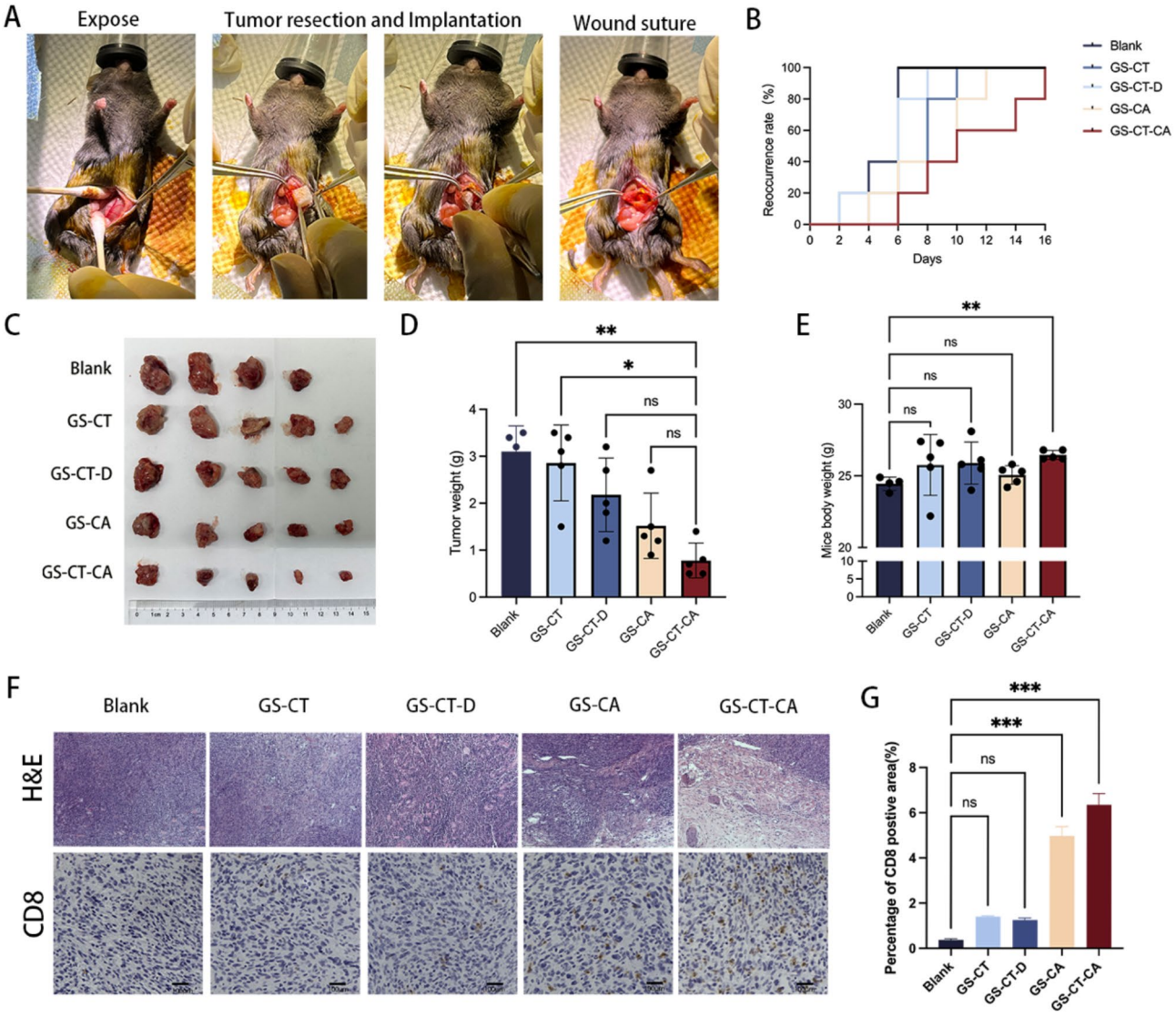

Fig. 6. Treatment of GS-CT-CA delayed residual tumor growth in intraperitoneal residual tumor model. (**A**) The procedures of tumor resection and implantation of CT-CA. (**B**) Tumor reoccurrence curves of mice treated with different combinations. (**C**) Tumors from mice at 16 days after surgery. (**D**) Tumor weight of different groups. (**E**) Mouse body weight after the removal of tumors on day 16. (**F**) H&E and CD8 staining of excised tumor. (**G**) Quantification of CD8 expression in tumour tissues. The data represent the mean ± SEM. ns, not significant; $^{**}P < 0.01$; $^{***}P < 0.001$. Blank, no treatment; GS-CT, gelatin sponge carrying CT; GS-CT-D, gelatin sponge carrying CT and DMSO; GS-CA, gelatin sponge carrying Cur and Apa; GS-CT-CA, gelatin sponge carrying Cur- and Apa-loaded CT.

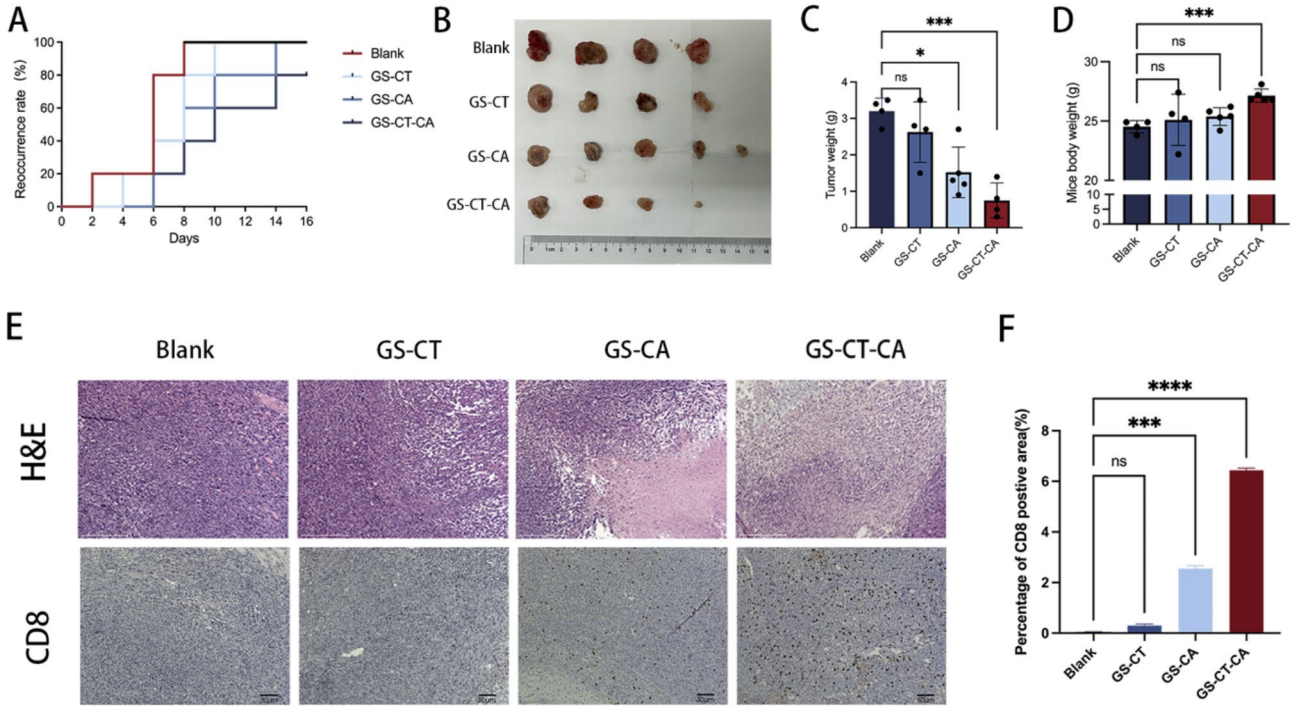

Fig. 7. GS-CT-CA delayed residual tumor growth in subcutaneous tumor model. (**A**) Tumor reoccurrence curve of mice treated with different combinations. (**B**) Tumor weight of different groups on day 16. (**C**) Mouse body weight after the removal of tumors on day 16. (**D**) Mouse body weight after the removal of tumors on day 16. (**E**) H&E and CD8 staining of excised tumor. (**F**) Quantification of CD8 expression in tumour tissues. The data represent the mean ± SEM. ns, not significant; $^{**}P < 0.01$; $^{***}P < 0.001$. Blank, no treatment; GS-CT, gelatin sponge carrying CT; GS-CA, gelatin sponge carrying Cur and Apa; GS-CT-CA, gelatin sponge carrying Cur- and Apa-loaded CT.

Data availability

All data generated or analysed during this study are included in this published article.

Received: 4 December 2024; Accepted: 7 April 2025
Published online: 11 May 2025

References

1. Tran, K. B. et al. The global burden of cancer attributable to risk factors. 2010-19: A systematic analysis for the global burden of disease study 2019. *Lancet* **400**, 563–591. https://doi.org/10.1016/s0140-6736(22)01438-6 (2022).
2. Chen, Z. et al. Surgical stress and cancer progression: The twisted Tango. *Mol. Cancer* **18**, 132. https://doi.org/10.1186/s12943-019-1058-3 (2019).
3. Pennathur, A. et al. Definition and assessment of high risk in patients considered for lobectomy for stage I non-small cell lung cancer: The American association for thoracic surgery expert panel consensus document. *J. Thorac. Cardiovasc. Surg.* **162**, 1605–1618e1606. https://doi.org/10.1016/j.jtcvs.2021.07.030 (2021).
4. Smyth, E. C., Nilsson, M., Grabsch, H. I., van Grieken, N. C. & Lordick, F. Gastric cancer. *Lancet* **396**, 635–648. https://doi.org/10.1016/s0140-6736(20)31288-5 (2020).
5. Kurahara, H. et al. Lung recurrence and its therapeutic strategy in patients with pancreatic cancer. *Pancreatology* **20**, 89–94. https://doi.org/10.1016/j.pan.2019.11.015 (2020).
6. Raskov, H., Orhan, A., Salanti, A. & Gögenur, I. Premetastatic niches, exosomes and circulating tumor cells: Early mechanisms of tumor dissemination and the relation to surgery. *Int. J. Cancer* **146**, 3244–3255. https://doi.org/10.1002/ijc.32820 (2020).
7. Foster, J. M., Zhang, C., Rehman, S., Sharma, P. & Alexander, H. R. The contemporary management of peritoneal metastasis: A journey from the cold past of treatment futility to a warm present and a bright future. *CA Cancer J. Clin.* **73**, 49–71. https://doi.org/10.3322/caac.21749 (2023).
8. Hasegawa, Y. et al. Fibroblast growth factor-impregnated collagen-gelatin sponge improves keratinocyte sheet survival. *Tissue Eng. Part. A* **28**, 373–382. https://doi.org/10.1089/ten.TEA.2021.0138 (2022).
9. Ranjbar, J. et al. Novel Chitosan/gelatin/oxidized cellulose sponges as absorbable hemostatic agents. *Cellulose* **28**, 3663–3675. https://doi.org/10.1007/s10570-021-03699-9 (2021).
10. Xie, X. et al. Conjugate electrospun 3D gelatin nanofiber sponge for rapid hemostasis. *Adv. Healthc. Mater.* **10**, e2100918. https://doi.org/10.1002/adhm.202100918 (2021).
11. Rohanizadeh, R., Swain, M. V. & Mason, R. S. Gelatin sponges (Gelfoam) as a scaffold for osteoblasts. *J. Mater. Sci. Mater. Med.* **19**, 1173–1182. https://doi.org/10.1007/s10856-007-3154-y (2008).
12. Sun, Y. et al. A natural polyphenol-functionalized Chitosan/gelatin sponge for accelerating hemostasis and infected wound healing. *Biomater. Sci.* **11**, 2405–2418. https://doi.org/10.1039/d2bm02049a (2023).
13. Hajosch, R. et al. A novel gelatin sponge for accelerated hemostasis. *J. Biomed. Mater. Res. B Appl. Biomater.* **94**, 372–379. https://doi.org/10.1002/jbm.b.31663 (2010).

14. Wang, W., Li, M., Wang, L., Chen, L. & Goh, B. C. Curcumin in cancer therapy: Exploring molecular mechanisms and overcoming clinical challenges. *Cancer Lett.* **570**, 216332. https://doi.org/10.1016/j.canlet.2023.216332 (2023).
15. Patiño-Morales, C. C. et al. Curcumin stabilizes p53 by interaction with NAD(P)H: Quinone oxidoreductase 1 in tumor-derived cell lines. *Redox Biol.* **28**, 101320. https://doi.org/10.1016/j.redox.2019.101320 (2020).
16. Liu, L. et al. The effect of Curcumin on multi-level immune checkpoint Blockade and T cell dysfunction in head and neck cancer. *Phytomedicine* **92**, 153758. https://doi.org/10.1016/j.phymed.2021.153758 (2021).
17. Shafabakhsh, R. et al. Targeting regulatory T cells by Curcumin: A potential for cancer immunotherapy. *Pharmacol. Res.* **147**, 104353. https://doi.org/10.1016/j.phrs.2019.104353 (2019).
18. Zhao, G. J. et al. Curcumin inhibits suppressive capacity of naturally occurring CD4 + CD25 + regulatory T cells in mice in vitro. *Int. Immunopharmacol.* **14**, 99–106. https://doi.org/10.1016/j.intimp.2012.06.016 (2012).
19. Rahiman, N., Markina, Y. V., Kesharwani, P., Johnston, T. P. & Sahebkar, A. Curcumin-based nanotechnology approaches and therapeutics in restoration of autoimmune diseases. *J. Control Release* **348**, 264–286. https://doi.org/10.1016/j.jconrel.2022.05.046 (2022).
20. Mortezaee, K. et al. Mechanisms of apoptosis modulation by Curcumin: Implications for cancer therapy. *J. Cell. Physiol.* **234**, 12537–12550. https://doi.org/10.1002/jcp.28122 (2019).
21. Yavarpour-Bali, H., Ghasemi-Kasman, M. & Pirzadeh, M. Curcumin-loaded nanoparticles: A novel therapeutic strategy in treatment of central nervous system disorders. *Int. J. Nanomed.* **14**, 4449–4460. https://doi.org/10.2147/ijn.S208332 (2019).
22. Wing-Fu, L., Eric, M. H. & Wing-Tak, W. A gel-forming clusteroluminogenic polymer with tunable emission behavior as a sustained-release carrier enabling real-time tracking during bioactive agent delivery. *Appl. Mater. Today* **21**, 100876. https://doi.org/10.1016/j.apmt.2020.100876 (2020).
23. Wing-Fu, L. et al. A self-indicating cellulose-based gel with tunable performance for bioactive agent delivery. *J. Drug Deliv. Sci. Technol.* **63**, 102428. https://doi.org/10.1016/j.jddst.2021.102428 (2021).
24. Obireddy, S. R. & Lai, W. F. Preparation and characterization of 2-hydroxyethyl starch microparticles for co-delivery of multiple bioactive agents. *Drug Deliv.* **28**, 1562–1568. https://doi.org/10.1080/10717544.2021.1955043 (2021).
25. Lai, W. F. & He, Z. D. Design and fabrication of hydrogel-based nanoparticulate systems for in vivo drug delivery. *J. Control Release* **243**, 269–282. https://doi.org/10.1016/j.jconrel.2016.10.013 (2016).
26. Lai, W. F. et al. A biocompatible and easy-to-make polyelectrolyte dressing with tunable drug delivery properties for wound care. *Int. J. Pharm.* **566**, 101–110. https://doi.org/10.1016/j.ijpharm.2019.05.045 (2019).
27. Lai, W. F., Susha, A. S. & Rogach, A. L. Multicompartment microgel beads for co-delivery of multiple drugs at individual release rates. *ACS Appl. Mater. Interfaces* **8**, 871–880. https://doi.org/10.1021/acsami.5b10274 (2016).
28. Lai, W. F. & Wong, W. T. Design of polymeric gene carriers for effective intracellular delivery. *Trends Biotechnol.* **36**, 713–728. https://doi.org/10.1016/j.tibtech.2018.02.006 (2018).
29. Lai, W. F., Reddy, O. S., Zhang, D., Wu, H. & Wong, W. T. Cross-linked Chitosan/lysozyme hydrogels with inherent antibacterial activity and tuneable drug release properties for cutaneous drug administration. *Sci. Technol. Adv. Mater.* **24**, 2167466. https://doi.org/10.1080/14686996.2023.2167466 (2023).
30. Lai, W. F., Reddy, O. S., Law, L., Wu, H. & Wong, W. T. A self-indicating and antibacterial gelatine-chitosan blended hydrogel enabling real-time quality control and sustained bioactive agent delivery. *RSC Adv.* **13**, 11865–11873. https://doi.org/10.1039/d2ra06802h (2023).
31. Obireddy, S. R. & Lai, W. F. ROS-generating amine-functionalized magnetic nanoparticles coupled with carboxymethyl chitosan for pH-responsive release of doxorubicin. *Int. J. Nanomed.* **17**, 589–601. https://doi.org/10.2147/IJN.S338897 (2022).
32. Boddu, A., Obireddy, S. R., Zhang, D., Rao, K. & Lai, W. F. ROS-generating, pH-responsive and highly tunable reduced graphene oxide-embedded microbeads showing intrinsic anticancer properties and multi-drug co-delivery capacity for combination cancer therapy. *Drug Deliv.* **29**, 2481–2490. https://doi.org/10.1080/10717544.2022.2100512 (2022).
33. Zhang, Z. et al. Sandwich-like fibers/sponge composite combining chemotherapy and hemostasis for efficient postoperative prevention of tumor recurrence and metastasis. *Adv. Mater.* **30**, e1803217. https://doi.org/10.1002/adma.201803217 (2018).

Author contributions

Conception and design: Z.M., J.C., Acquisition of data: Z.M., J.C., Analysis and interpretation of data: C.Y. Y.S. and S.Z., Drafting the article: Z.M., O.S.R., K.L., Y.W., H.G. and F.W., Critically revising the article: all authors; Statistical analysis: S.X. and L.S., Reviewed submitted version of the manuscript: all authors; Funding acquisition: A.H. and B.C. Approved the final version of the manuscript on behalf of all authors: D.Z., Study supervision: W.L., G.W. and D.Z.

Declarations

Competing interests

The authors declare no competing interests.

Statements of accordance and arrive guidelines

Accordance: We confirmed that all experiments in this study were performed in accordance with the relevant guidelines and regulations. Arrive: All the procedure of the study is followed by the ARRIVE guidelines.

Additional information

Correspondence and requests for materials should be addressed to W.-F.L., G.-Q.W. or D.-H.Z.